Harsh imaging techniques for shallow high resolution seismic data

David C. Henley

ABSTRACT

There is increasing interest in the use of high resolution seismic methods to image the shallowest layers of the earth in pursuit of various objectives, including bedrock features, buried cultural structures such as pipelines, and even paleontological or archaeological anomalies. Often the surveys are carried out with some difficulty under non-ideal conditions, and the resulting data may be quite poor in quality and sparse in fold or coverage. Described here are the results of applying a number of unconventional and rather "harsh" techniques to image two components of a 3-C seismic survey carried out in the vicinity of archaeological ruins in Belize during the summer of 2000 with the objective of locating subsurface disturbances consistent with various interesting archaeological features. While ambiguities remain in the identification of the 3-C components, images are presented for both 'vertical' and 'inline' components of the survey, which seem to show similar features at roughly coincident locations on the line.

INTRODUCTION

Shallow, high resolution seismic data frequently present special difficulties for obtaining usable images because they are often acquired with small portable seismic acquisition systems having a limited number of channels, using inexpensive surface sources like sledge hammer impacts or Betsy projectile guns. The consequence of the channel limitation is often small fold for combating noise, uneven binning, and either a limited source-receiver offset range or inadequate spatial sampling. The consequence of using a surface source, on the other hand, is often a high level of source-generated noise on the records. Faced with handicaps like this, a seismic processor must sometimes resort to unconventional, sometimes controversial procedures that would rarely be applied to more conventional seismic data. Justification for such methods comes from the objectives for the imaging of the data, which can differ from the imaging objectives for more conventional data. Whereas seismic "character", including broadband amplitude and phase information is the goal of most conventional imaging, seismic "structure" is the goal of much shallow, high resolution work. In this context, *any* image is useful if it helps delineate the subsurface structure, regardless of its bandwidth or phase characteristics. With this somewhat relaxed objective in mind, some relatively radical processing strategies can sometimes help extract an image from marginal data.

The 3-C survey from Belize (Stewart, 2000) exhibits all of the data characteristics described above and thus was subjected to techniques seldom used except on problem data sets, such as the 1998 Shaganappi geotechnical survey (Henley, 1999). To illustrate the difficulties, Figure 1 shows receiver gathers from the tentatively identified 'vertical' component of the Belize survey, while Figure 2 shows

comparable receiver gathers from the 'inline' component. Almost all the visible energy on either set of gathers is linear source-generated noise; and in fact, it is difficult to determine by eye which component is which, based on these gathers. Only during processing was the current tentative assignment of these components as 'vertical' or 'inline' adopted, and this identification disagrees with that assumed in the field—a serious quandary for interpretation. In all likelihood, however, the traces for each component contain significant energy from both components, and the processing flow determines whether the vertical (P-P reflections) or inline (P-S conversions) are properly imaged for either data set.

The first of the "harsh" techniques to be applied to these data is multiple passes of coherent noise attenuation in which very 'aggressive' low-cut filter parameters are chosen. In order to increase the coherence of the source-generated noise for effective attenuation, the data are sorted to shot gathers and made into a single supergather as shown in Figure 3. Several modes of linear noise apparent on the supergather can be addressed using radial trace dip filters (Henley, 1999). These passes were applied for three different apparent velocities using a steep-rolloff low-cut filter with -6 dB point at 80 Hz (the data were recorded with .25 ms samples and contain frequencies of at least 300 Hz). The filtered supergather is shown in Figure 4, where several sub-horizontal events are now visible. These traces were then re-sorted into a common-offset supergather as shown in Figure 5. This display format proved to be the most useful for analysing NMO. Experimentation with a broad range of stacking velocities led to the choice of a stacking velocity function which appears to correct most of the event moveout, as shown in Figure 6. The subsequent CDP stack in Figure 7 displays coherent events in the shallow portion of the section, but the event coherence is significantly disturbed. The alternate-trace amplitude fluctuations visible to the left of centre may be due to variations in trace fold of alternate bins, or to trace polarity reversals within the gathers, if these data ultimately prove to be 'inline' data rather than the currently assumed 'vertical' component.

Whatever the cause of the visible discontinuities and fluctuations, a stacked section like that in Figure 7 is a situation for which the unconventional "harsh" technique called "wavefront healing" (Henley, 2000) is suited. After a single step of wavefront healing, the coherence improves markedly, as shown in Figure 8. Comparison of Figures 7 and 8 confirms that the events in 8 are not phantoms created by the processing, as they are actually present in 7. The wavefield in Figure 8 is continuous enough to migrate, and the result of post-stack Kirchhoff migration is shown in Figure 9. At this point the data are laterally stable enough to apply a modest predictive deconvolution to shorten the event wavelets and broaden the band. The result of this is the 'vertical' component image in Figure 10. There are several features of interest in this image. The event at 12 ms exhibits interesting breaks in its continuity at CDP's 20000-20015 and 20090-20125. The break at 20090-20125 is especially interesting because of the sag in the event between these points and the abrupt edges of the break with slight uplift at either edge.

Although the above description of the processing flow for these data is straightforward, the processing *sequence* was the subject of much experimentation

before the flow was adopted. Every attempt was made to avoid wavefront healing, but Kirchhoff migration was incapable on its own of creating a useful wavefield image without healing as a pre-processing step. Likewise, attempts were made to place deconvolution earlier in the flow; but the data are insufficiently stable to support a laterally coherent predictive deconvolution until after migration. Remarkably, the coherent higher-frequency information appears to survive the wavefront healing and migration, and is restored by a very modest predictive deconvolution operation (16 ms operator, 0.1 stability factor). Note the lateral coherence of the reflection events in spite of the fact that the deconvolution operator was derived and applied individually for each trace.

The presumed 'inline' horizontal component of this data set was treated in a similar fashion, but with some extra considerations. Experimentation led to the conclusion that these data were contaminated with even stronger noise than the 'vertical' component data, and that, except for the direct P arrival, this noise typically had a lower velocity than that on the vertical data. The noise reduction, as in the 'vertical' component case, was performed on a supergather made from the shot gathers. In this case, however, linear moveout corresponding to the velocity of the direct P arrival was applied to the shot gathers prior to merging them into the supergather to make the various low velocity noise components easier to identify for removal with radial dip filtering. After filtering out noise modes at three different linear velocities with a low-cut of 80 Hz, the horizontal energy in the supergather (likely direct P arrival energy) was attenuated using a radial trace dip filter. The raw inline supergather appears in Figure 11, while the supergather after linear moveout is shown in Figure 12. The removal of the first three noise modes yields Figure 13, while the result of the additional filter pass to attenuate the horizontally aligned P-wave energy appears in Figure 14.

Restoring the linear moveout to the supergather and sorting the traces to a common-offset supergather results in Figure 15, in which reflection event moveout is now apparent. Interestingly, this moveout does not appear to be hyperbolic. Nevertheless, application of hyperbolic NMO corresponding to a velocity function with *very* low velocities (150 m/s, compared to 420 m/s for the vertical data) results in reasonable event alignment on the common-offset gathers, as shown in Figure 16. In this figure, the non-hyperbolic nature of the event moveout is evident at the longest offsets. As well, some of the shallower events at longer offsets in Figure 15, likely corresponding to 'vertical' energy leaking into the 'inline' component, have been stretched beyond recognition and muted. As with the previous component, a wide range of NMO velocities was tested, including those consistent with vertical P-wave energy. While the P-consistent velocities can stack these data successfully, presumably due to the leakage of P-wave energy into this component, the most compelling event alignment on the common-offset gathers is that shown in Figure 16, where very low-velocity NMO has been applied. Comparison with Figure 15 is somewhat deceptive, since the most prominent shallow coherent events in that figure have been stretched excessively and muted; the most prominent coherent events in Figure 16 actually originate as somewhat deeper, barely visible events in Figure 15, with considerably more moveout. This identification was actually made in practice by

applying NMO in two smaller steps, at a higher velocity, in order to observe the incremental NMO correction on the events.

Because inline component data are presumed to be P-S converted wave energy, it was no surprise to find that the presumed 'inline' traces do not stack very well in common-CDP bins. Instead, new bins were created to gather traces at P-S conversion points. The large difference in NMO velocities required to correct the vertical and inline data (420 m/s vs 150 m/s) implies a Vp/Vs of 3:1 or higher, which further implies a conversion point very close to the receiver position for each source-receiver pair. Accordingly, CCP bin positions ranging from 2/3 to 7/8 of the source-receiver distance were tried for stacking the inline data. Based on the coherence of the resulting stack, the 5/6 bin position resulted in the most coherent reflections for the 20-60 ms time zone. A single bin position is optimum only for a very limited range of reflection depths. No attempt was made, however, to use any dynamic CCP binning scheme, since only a narrow zone of reflections was of interest.

A further inconsistency should be noted here: the polarity of inline component data is expected to reverse on opposite sides of the source location, but only weak evidence of polarity reversal could be seen on any of the raw receiver gathers for either 'vertical' or 'inline' component data, or, indeed, on any of the noise-attenuated gathers for either data set. Nevertheless, an attempt was made to process the 'inline' data as if the polarity reversal was present. When the polarity reversal was included, the data seemed to stack best at the 3/4 CCP position, but the lateral position of anomalies in the reflections changed relative to the original 5/6 CCP stack without polarity reversal. The character of the reflection seemed less consistent along the length of the profile.

Figure 17 displays the stack of the inline data for the 5/6 CCP bin positions. While this section looks disappointingly random, an examination of it at low angle from the side reveals a number of faint sub-horizontal events possibly corresponding to reflections. As shown in Figure 18, application of two steps of low-velocity wavefront healing greatly enhances the event coherence, and the addition of Kirchhoff post-stack migration in Figure 19 leads to a credible band of reflections between about 20 and 80 ms. The final step, predictive deconvolution, using exactly the same parameters as for the 'vertical' component data, yields the surprising image in Figure 20. The very shallow energy in this figure is leakage of vertical component energy, which cannot be easily attenuated by stacking because it appears only on a few short offset traces. The band of energy between 30 and 80 ms, on the other hand, appears to be legitimate reflection energy. The most surprising aspect of this image is the significantly higher frequency of these reflections compared to those on the 'vertical' component image. This is consistent, however, with a very slow Vs value and dramatically illustrates the potential value of shear-wave or converted P-S data, as the vertical resolution of this image significantly exceeds that of Figure 10. Lateral discontinuities in the reflection event at 34 ms occur at CCP positions of 19995-20020 and 20090-20140. These breaks correlate reasonably well with those in the 12 ms reflection in Figure 10, although the gaps are somewhat wider, and the larger of the two has less distinct boundaries. The overall impression of Figure 20 is that its

vertical resolution exceeds that of Figure 10, but its lateral resolution is somewhat less. The latter may be due to the smearing effect of the additional wavefront healing step, or just to the uncertainty in the position of the CCP.

Finally, Figure 21 shows the alternate image for the 'inline' component, when polarity of traces is appropriately treated and the data are stacked at the 3/4 CCP position. All other processing, including parameter choice, is identical to that used to produce the image in Figure 20.

DISCUSSION

The images in Figures 10, 20, and 21 provide an intriguing picture of the Belize 3-C seismic survey. The images in Figures 10 and 20, in particular, seem consistent with a strong reflecting boundary at a depth of just under 2 metres, significantly laterally discontinuous at two or more locations. They also imply a Vp/Vs ratio of at least 3:1. In spite of the relative consistency of the two images with each other, significant difficulties exist with the data. The most serious of these is the apparent contradiction between the field identifications of the vertical and inline components and those adopted after considerable experimentation with processing and imaging techniques. Care has been taken to preclude the introduction of false coherent events into either data component. Because extreme measures have been taken to obtain the two images ("harsh" radial trace dip filtering, "harsh" wavefront healing, unorthodox processing sequence), however, the possibility exists that processing artefacts have intruded into these images. A more likely possibility, though, is that both vertical and inline horizontal wave energy are present in significant strength on traces of both components, and the choice of processing flow determines which wavefield is best imaged for a given data set. As noted earlier, the 'inline' component will yield a 'vertical' component image when processed with velocities appropriate to that component. If the 'inline' image does, indeed, originate from the actual vertical component data, the lack of a convincing trace polarity reversal at source positions would be more easily explained. Immediate further analysis of these data will include application of the complete 'inline' processing flow to the 'vertical' component data and vice versa, to attempt to resolve the component identification discrepancy.

CONCLUSIONS

This report presents a first look at the 3-C seismic data acquired in Belize. Because of the poor quality and sparse fold of the data, "harsh" processing techniques have been applied to obtain images presumed to be P-P reflection and P-S conversion images. While the resulting images seem consistent with each other and imply a rather extreme Vp/Vs value, there remain ambiguities in the data set that need to be further studied and resolved. The most important of these is simply the positive identification of which component is 'vertical' and which is 'inline', since the current processing results conflict with the field identification. Regardless of the ultimate resolution of this problem, there is not much doubt that the images in Figures 10 and 20 are legitimate representations of P-P reflections and P-S conversions, respectively. Images like those in Figures 10 and 20 should provide useful information to

archaeologists and others wishing to locate subsurface anomalies without invasive methods such as excavation.

ADDENDUM

Further tests were performed on these data after completion of the main body of this work. Specifically, the 'vertical' component data were processed using the same flow as the 'inline' component data, and vice-versa. It proved possible to image both the vertical wavefield and the inline horizontal wavefield from *both* data sets, although specific details of the images differed. The following observations were made: The vertical wavefield image was stronger and somewhat more coherent when formed from the 'vertical' component data, and the image was best with *no* polarity reversal of negative offset traces; while the vertical wavefield image formed from the 'inline' data was most coherent when polarity of negative offset traces *was* reversed. The inline wavefield image was somewhat higher in vertical resolution when formed from the 'inline' data, and seemed moderately more coherent when negative offset traces had reverse polarity; while the image formed from the 'vertical' data was somewhat lower in frequency and somewhat more coherent for *no* trace polarity reversal. The most consistent correlation of lateral anomalies on the images remains with 'vertical' data processed as vertical, with no polarity change, and 'inline' data processed as inline, with negative offset trace polarity reversal. Overall, these tests tend to support the initial adoption of the labels 'vertical' and 'inline' as used above in the main body of the report.

ACKNOWLEDGEMENTS

The author wishes to acknowledge CREWES staff and sponsors for support of this work. Special thanks are due to Henry Bland, Rob Stewart, and Pat Daley for extensive discussions about these data and processing methods.

REFERENCES

Henley, D.C., 1999, Demonstration of radial trace domain filtering on the Shaganappi 1998 2-D geotechnical survey, CREWES Research report, **11**, pp 787-803.

Henley, D.C., 2000, Wavefront healing operators for improving reflection coherence, CREWES Research report, **12**, pp

Stewart, R.R., 2000, Private communication.

FIGURES

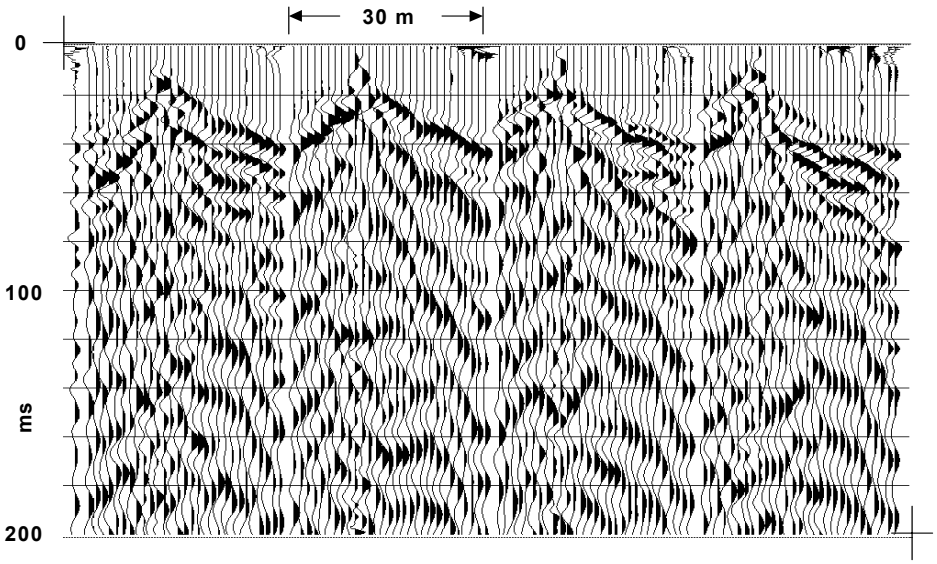

Figure 1. Presumed 'vertical' component receiver gathers from the 2000 Belize high resolution 3-C seismic survey.

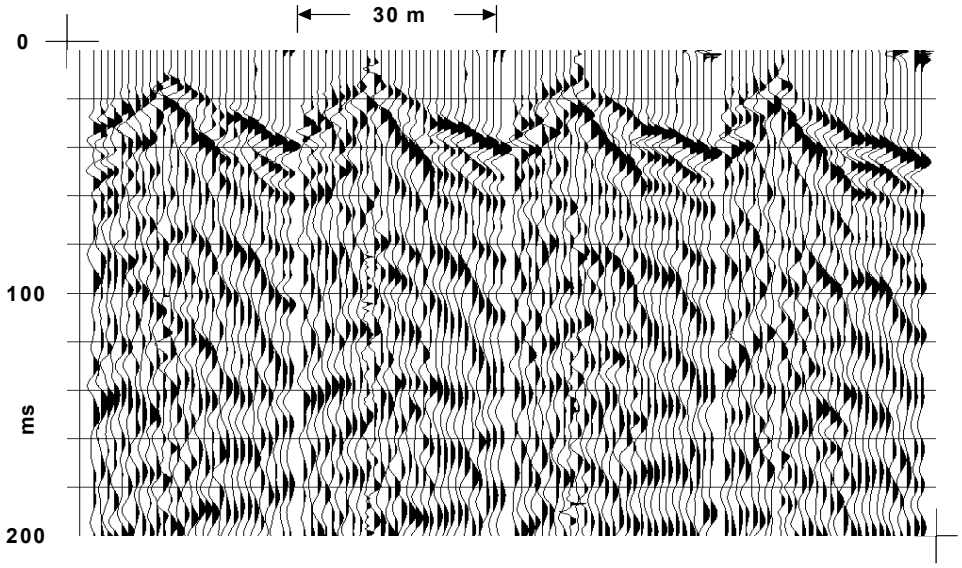

Figure 2. Presumed 'inline' horizontal component receiver gathers from the 2000 Belize high resolution 3-C seismic survey.

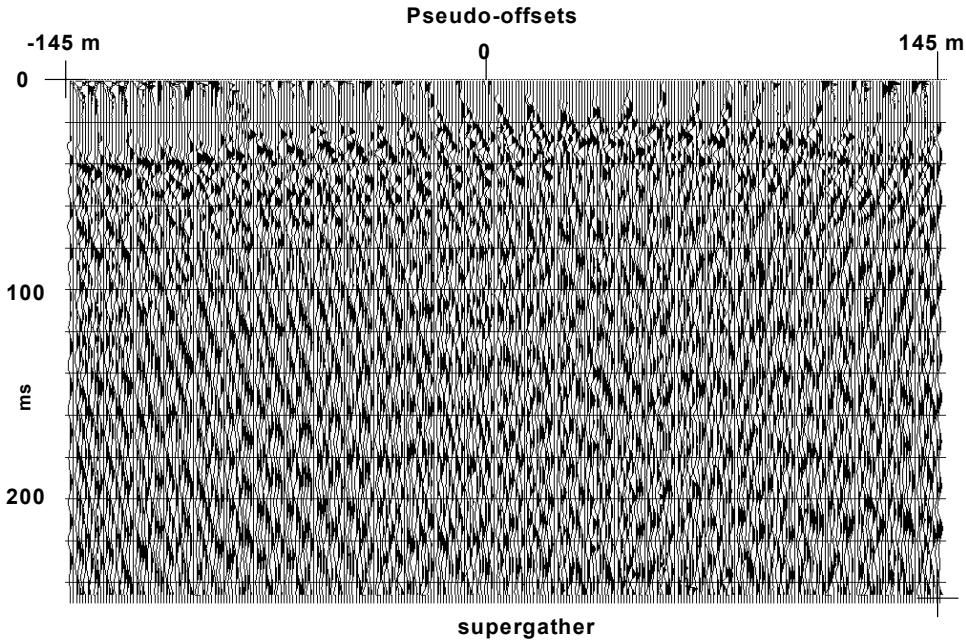

Figure 3. Supergather formed from 'vertical' component traces sorted by shot and signed source-receiver offset. Several modes of linear noise are evident.

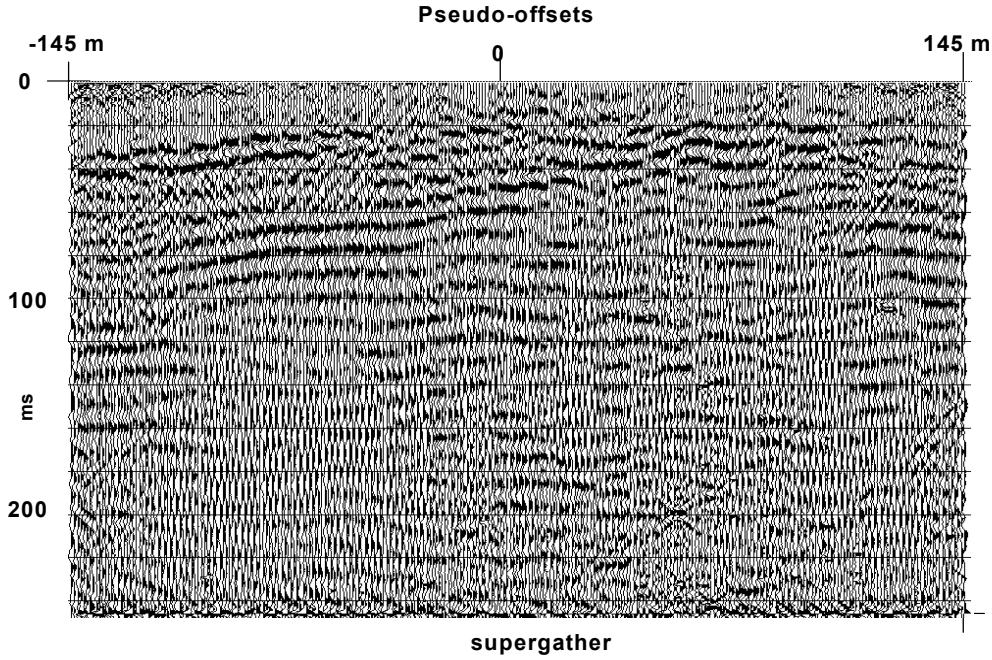

Figure 4. 'Vertical' component supergather after three passes of radial trace domain dip filtering, with low-cut of 80 Hz, to remove linear noise modes.

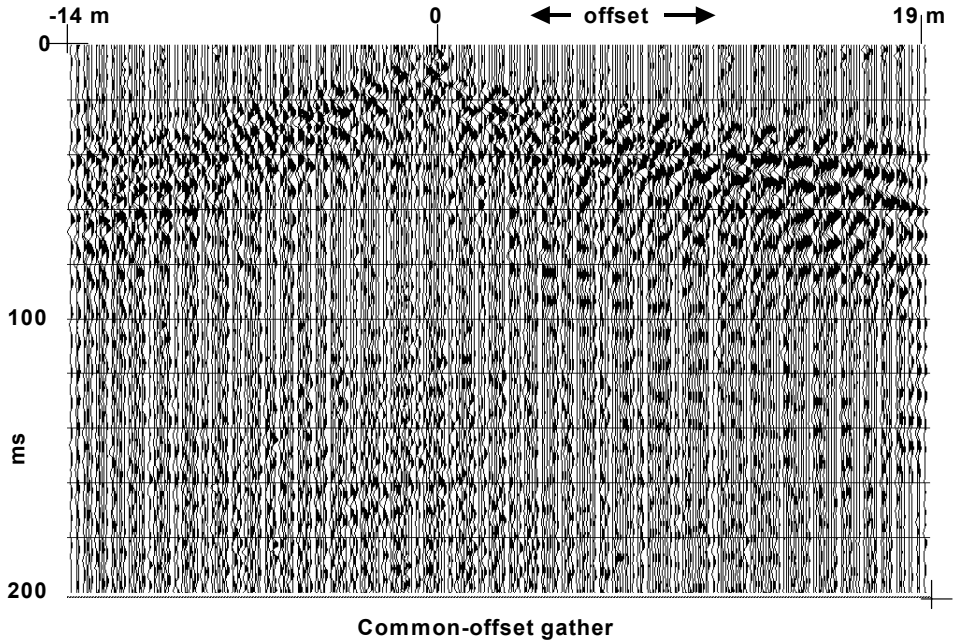

Figure 5. Common-offset supergather formed from filtered 'vertical' component traces sorted by source-receiver offset and source location. Vertical component moveout is evident.

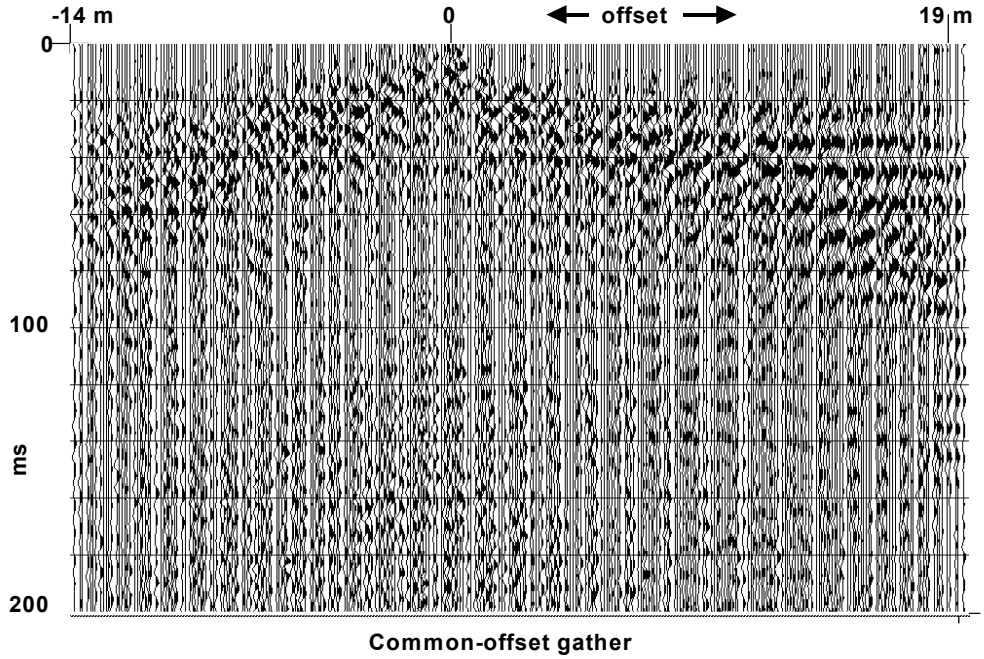

Figure 6. Common-offset 'vertical' component supergather after NMO correction using a velocity of 420 m/s.

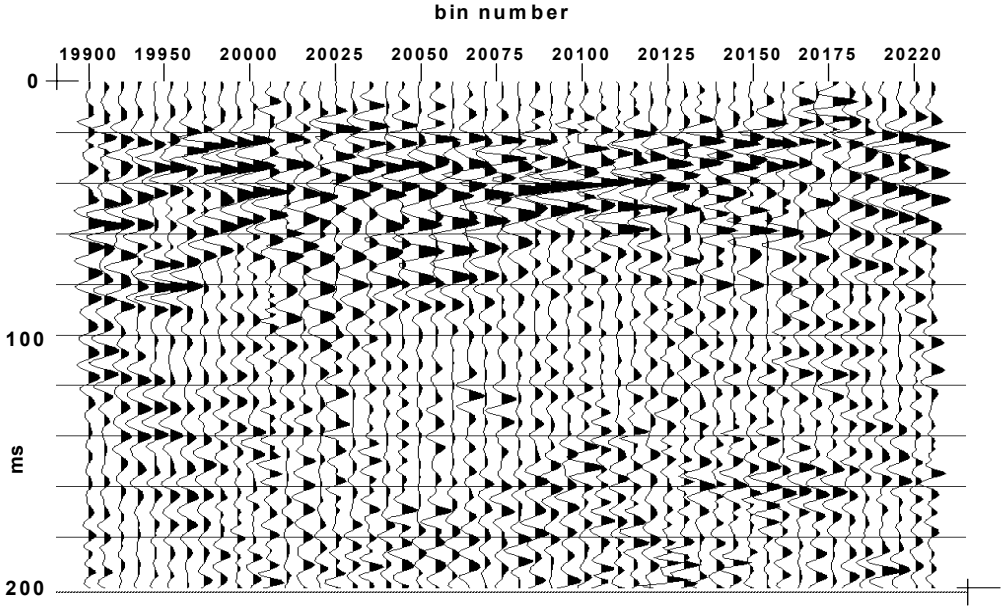

Figure 7. CDP stack of 'vertical' component data after NMO correction shown in Figure 6.The non-uniform CDP fold shows up as trace-to-trace amplitude and static variations.

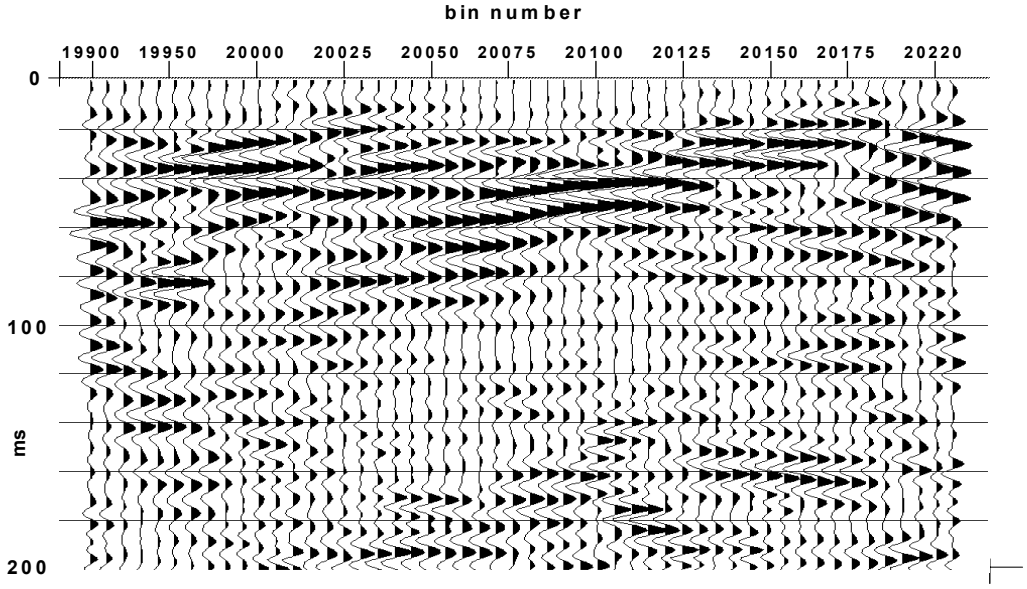

Figure 8. CDP stack of 'vertical' component data after the application of one pass of wavefront healing using the stacking velocity associated with time zero. Event continuity is greatly improved.

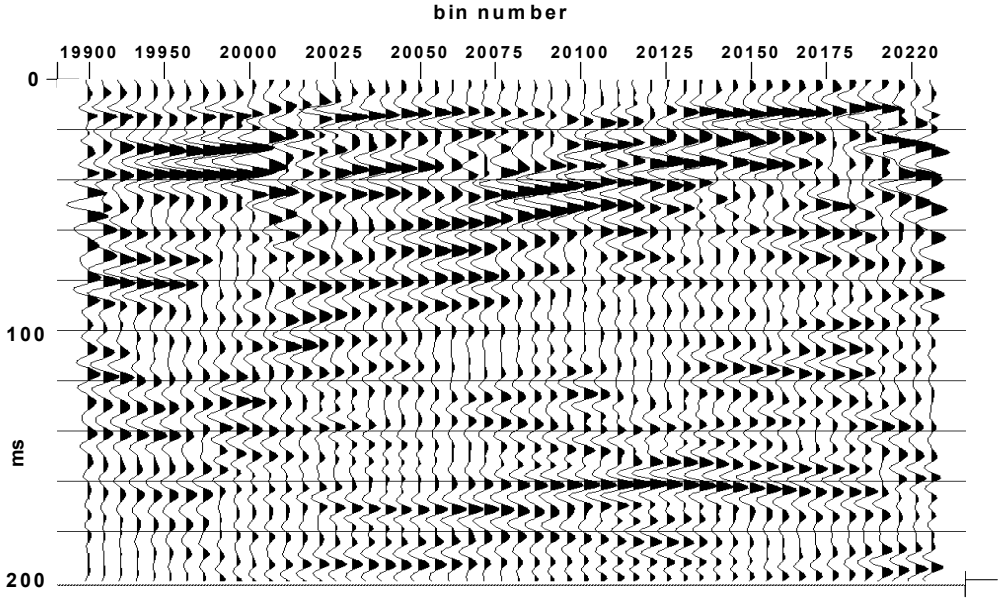

Figure 9. CDP stack of 'vertical' component data after wavefront healing and Kirchhoff migration using the stacking velocities.

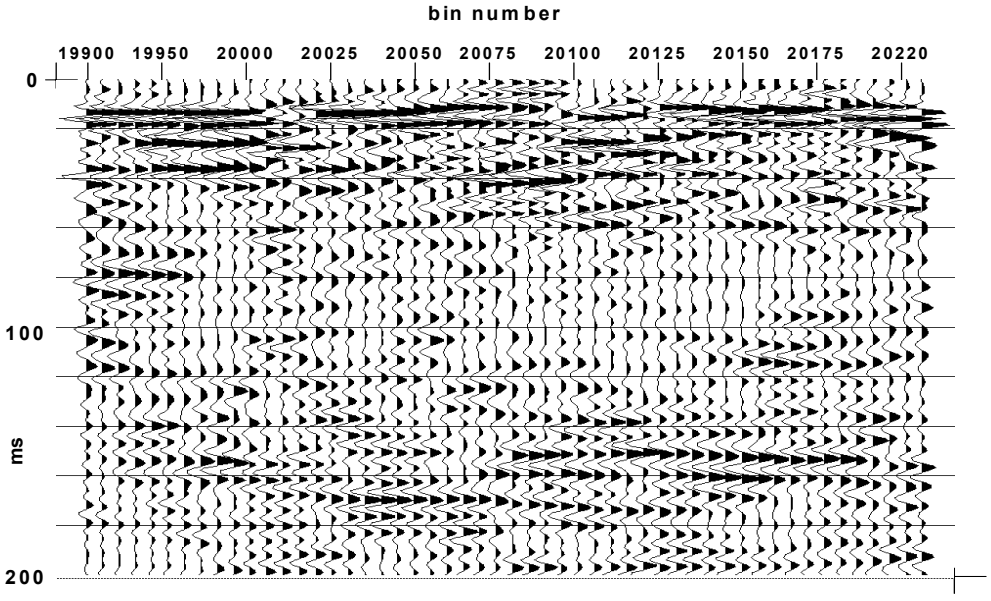

Figure 10. CDP stack of 'vertical' component data after wavefront healing, Kirchhoff migration, and predictive deconvolution.

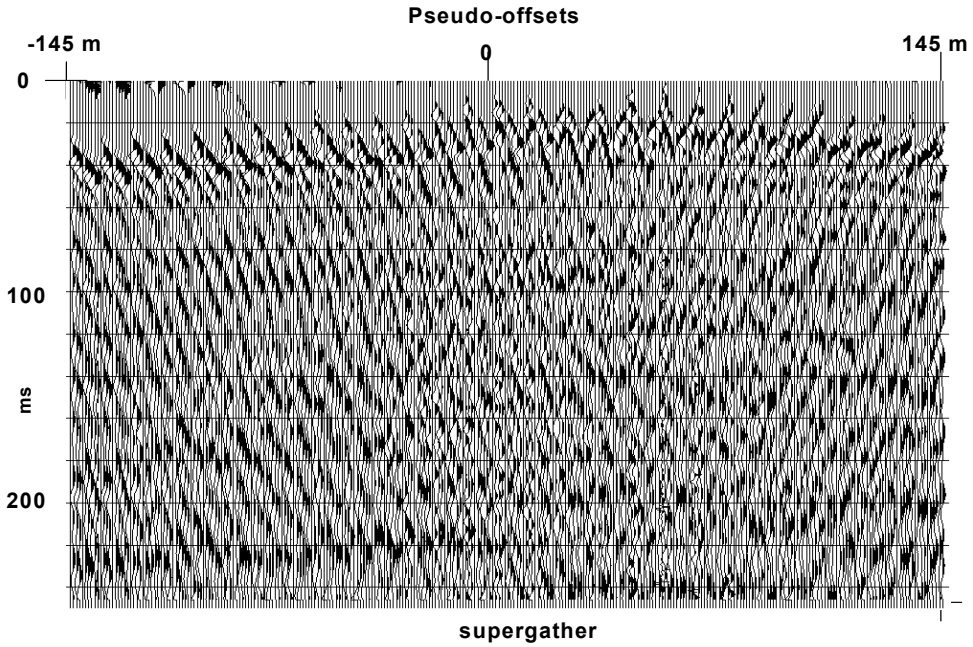

Figure 11. Supergather formed from 'inline' horizontal component traces sorted by shot and source-receiver offset. Many linear modes obvious.

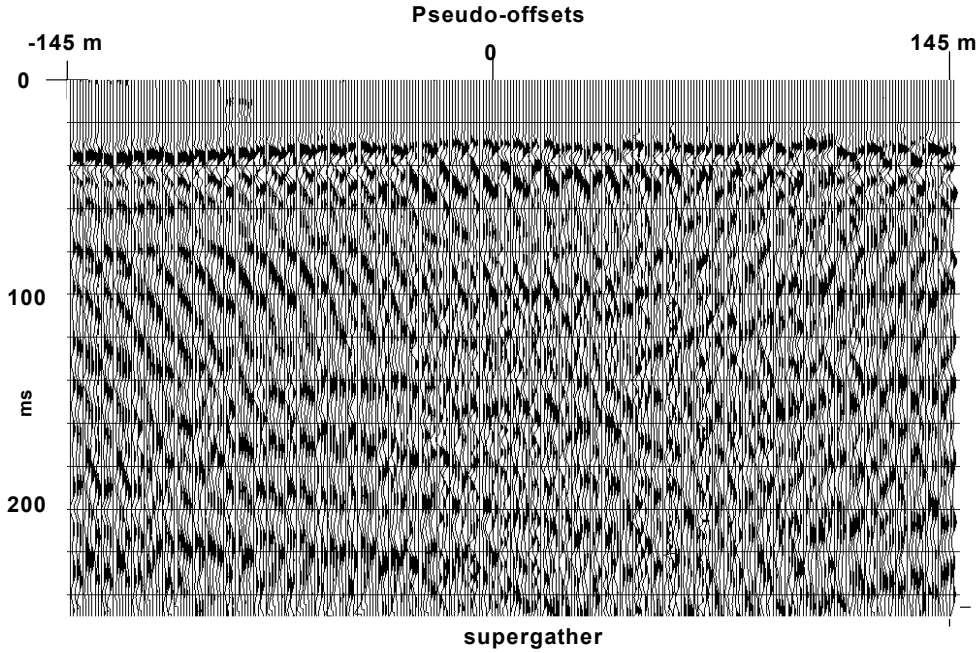

Figure 12. 'Inline' supergather after correction for linear moveout of 500 m/s (approximately the velocity of direct P-wave arrival).

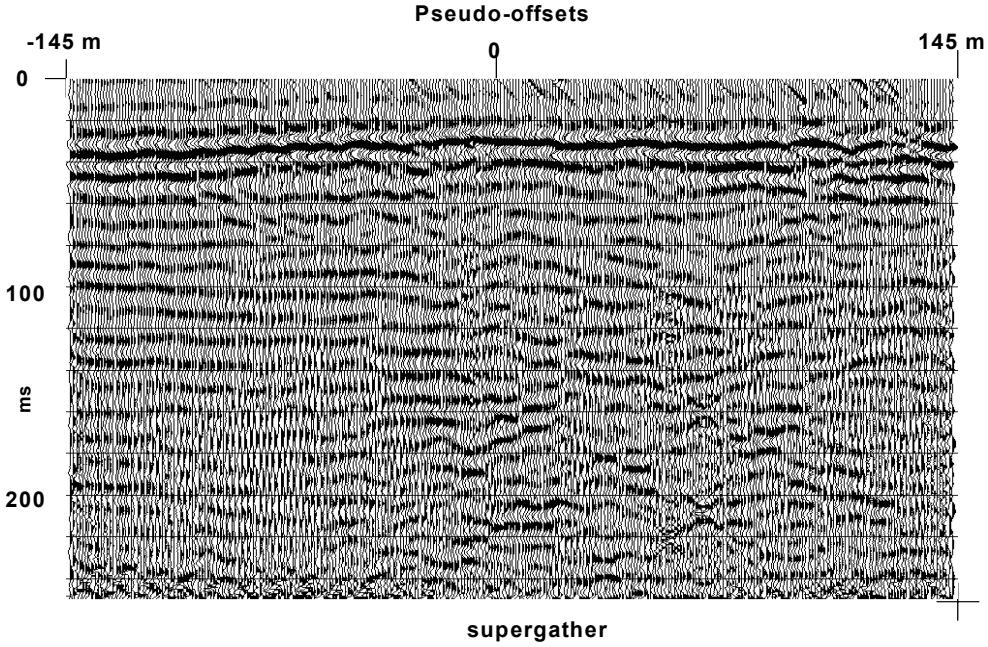

Figure 13. 'Inline' supergather after attenuation of three modes of linear noise with a low-cut of 80 Hz. Strong horizontal energy in this plot is 500 m/s direct P arrival energy, *not* reflection energy.

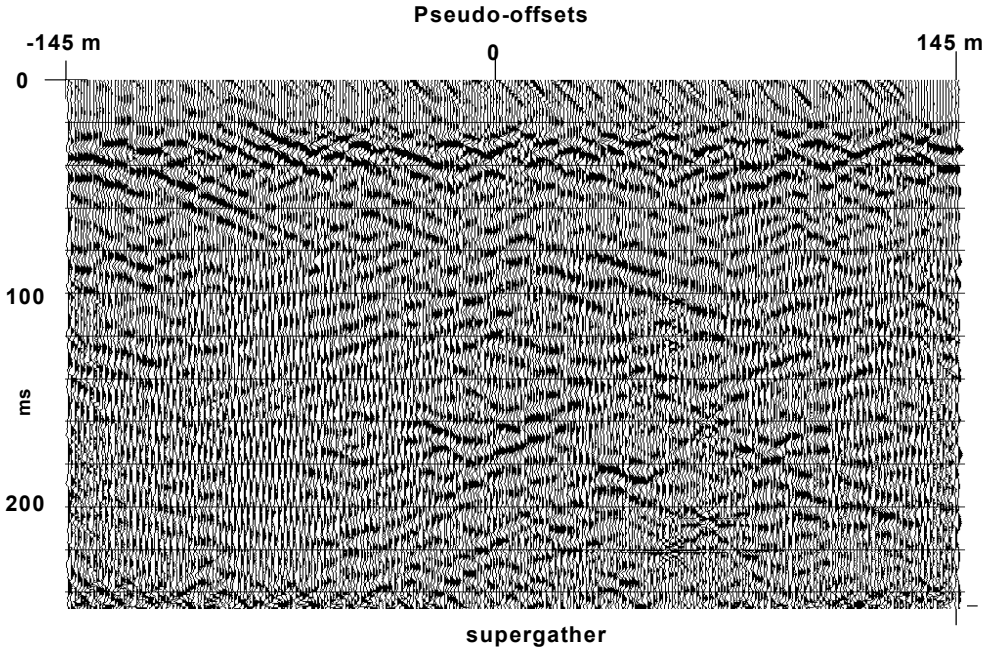

Figure 14. 'Inline' supergather after attenuation of direct P arrival energy. Linear moveout of 500 m/s must be restored to this supergather before re-sorting it to common-offset supergather.

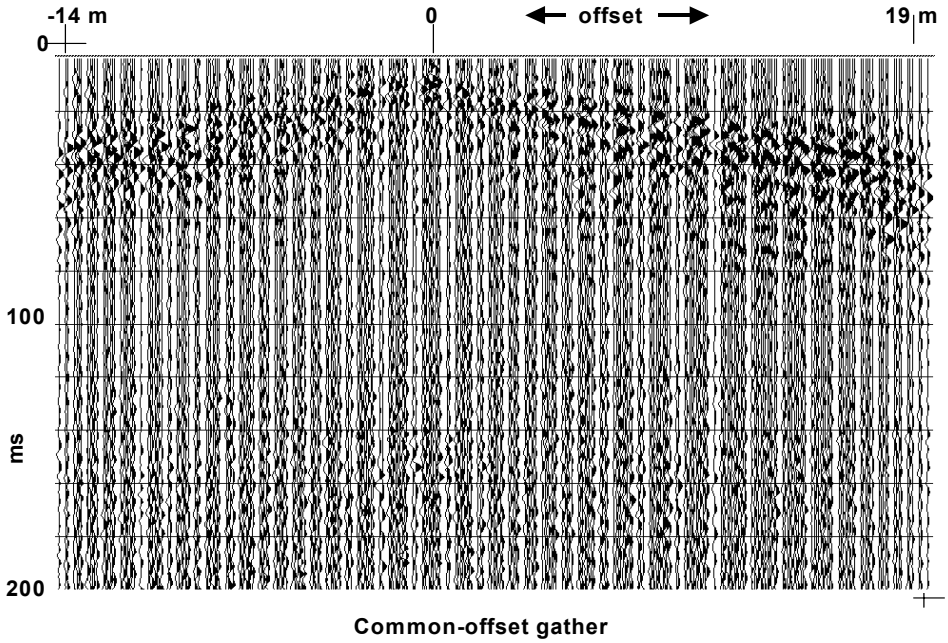

Figure 15. Common-offset supergather formed from filtered 'inline' component traces by sorting to source-receiver offset and shot location. More than one pattern of moveout is visible; moveout is *not* hyperbolic.

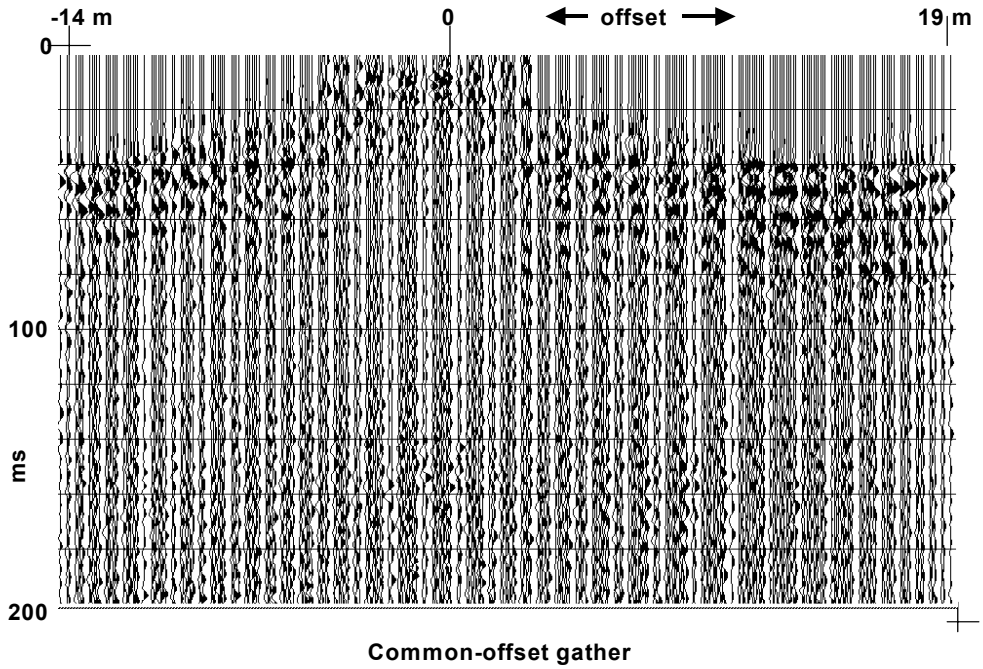

Figure 16. 'Inline' common_offset supergather after application of 150 m/s NMO. Very low velocity function has led to stretch muting of leaking shallow P-wave energy at longer offsets.

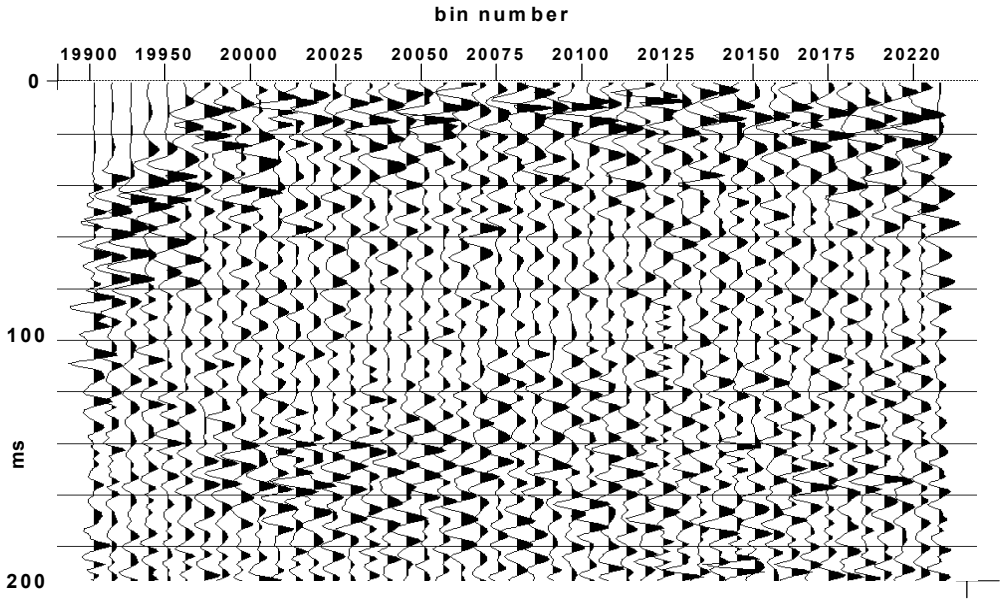

Figure 17. CCP stack of NMO-corrected 'inline' data using CCP locations of 5/6 source-receiver distances. Horizontal events can be faintly seen at about 10 ms, 50 ms, 110 ms.

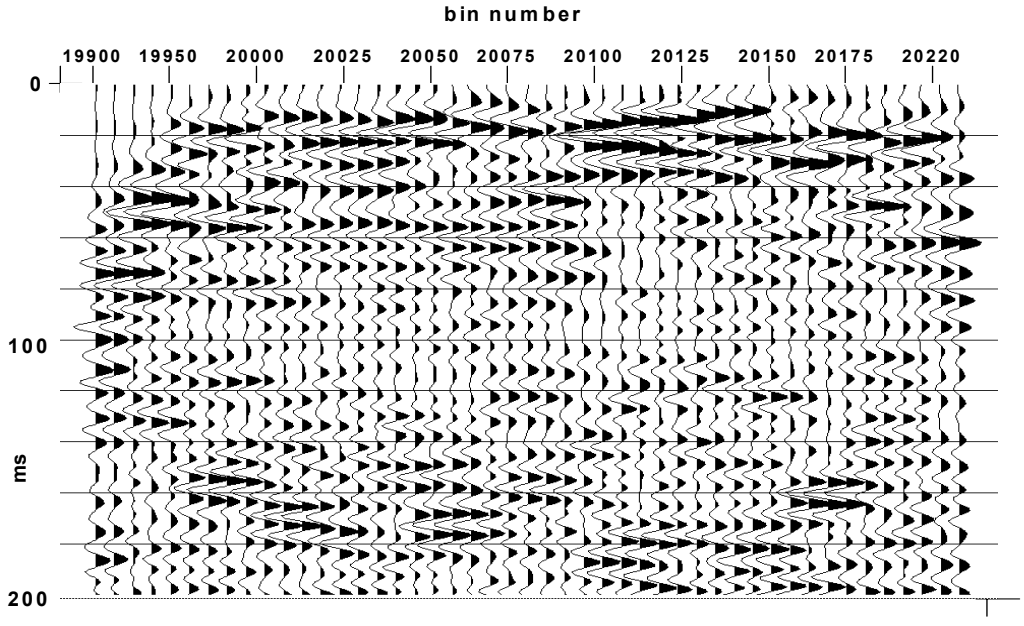

Figure 18. CCP stack of 'inline' data after two passes of wavefront healing using the velocity at time zero in the NMO function. Event coherence is much better than in Figure 17.

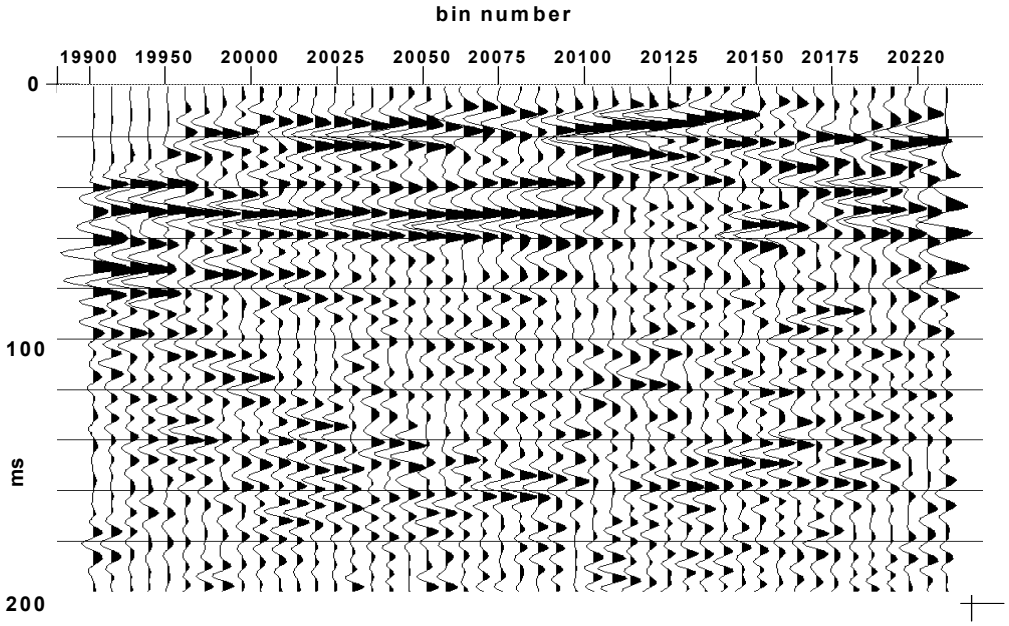

Figure 19. CCP stack of 'inline' data after wavefront healing and Kirchhoff migration using the NMO velocity function.

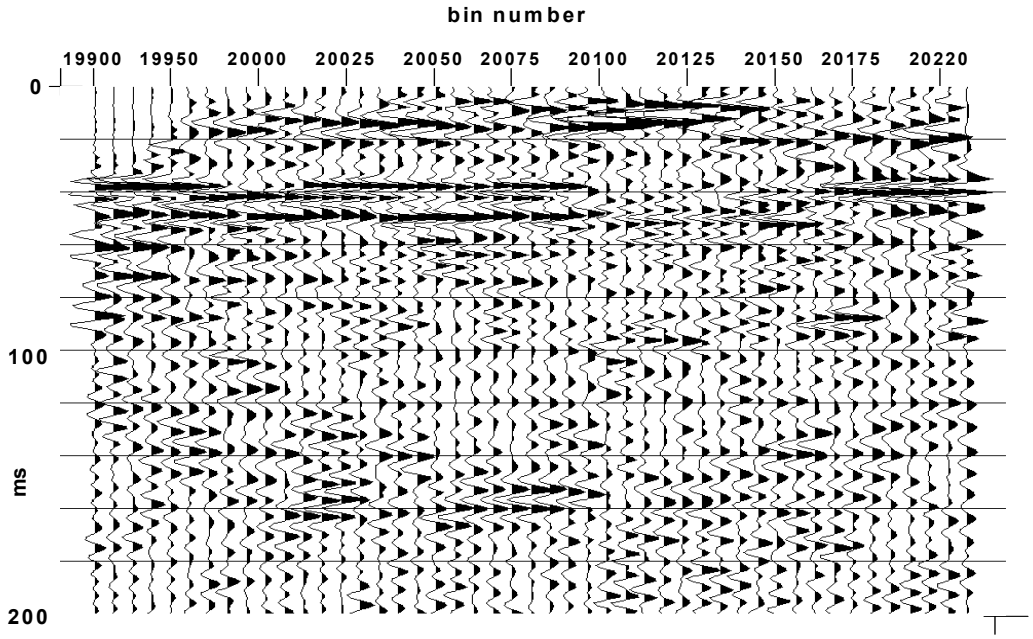

Figure 20. CCP stack of 'inline' component after wavefront healing, Kirchhoff migration and predictive deconvolution. Remarkably high frequencies are recovered for the events between 40 and 60 ms.

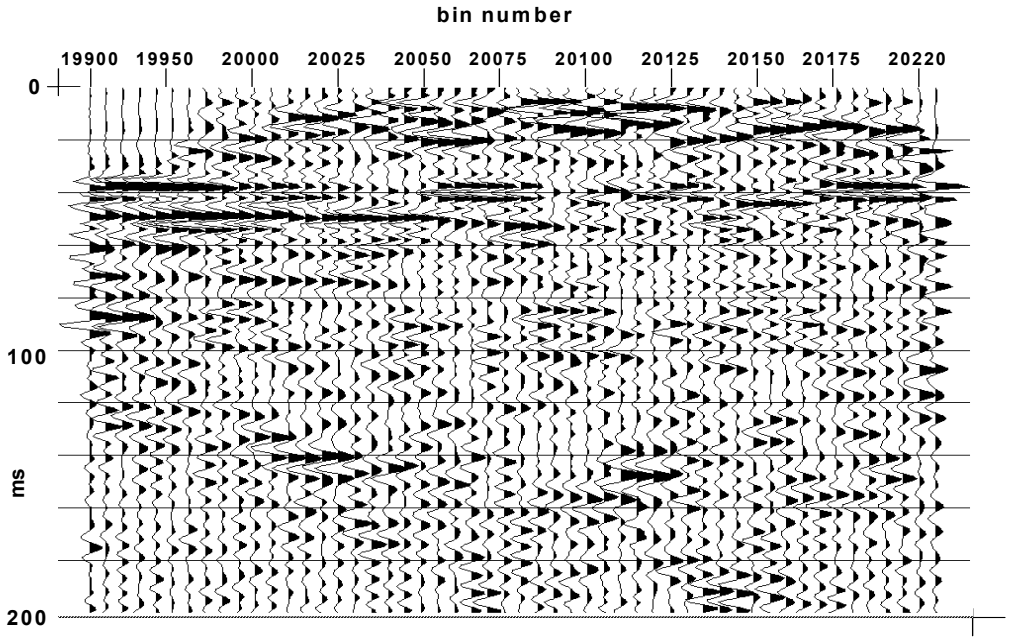

Figure 21. Alternate CCP section formed by negating the polarity of all negative source-receiver offset traces and stacking on the 3/4 source-receiver distance CCP. All other processing is the same as for Figure 20.